Wiley
Journal of Food Quality
Volume 2024, Article ID 7313214, 13 pages
https://doi.org/10.1155/2024/7313214

WILEY

Research Article

Application of Hyperspectral Imaging for Watermelon Seed Classification Using Deep Learning and Scoring Mechanism

Hengnian Qi,[1] **Mengbo He**,[1] **Zihong Huang**,[1] **Jianfang Yan**,[2] **and Chu Zhang**[1]

[1]*School of Information Engineering, Huzhou University, Huzhou 313000, China*
[2]*Zhejiang Provincial Seed Management Station, Hangzhou 310020, China*

Correspondence should be addressed to Chu Zhang; chuzh@zjhu.edu.cn

Received 8 March 2024; Revised 7 May 2024; Accepted 14 May 2024; Published 29 May 2024

Academic Editor: Yuxia Fan

Watermelon seeds are a significant source of nutrition in the diet. To assess the potential of near-infrared hyperspectral imaging technology for swift and nondestructive identification of watermelon seed varieties, near-infrared hyperspectral imaging (NIR-HSI) technology was used. The Savitzky–Golay (SG) smoothing algorithm and standard normal variable (SNV) algorithm were combined to preprocess the extracted spectral data. The successive projections algorithm (SPA) was used to reduce the dimensionality of the spectral data. Subsequently, three deep learning models (LeNet, GoogLeNet, and ResNet) were used to classify 10 common watermelon seeds. SPA was used to reduce the dimensionality of hyperspectral data. In terms of full band, the ResNet model achieved a classification accuracy of 86.77% on the test set. By using characteristic bands, the GoogLeNet model achieved a classification accuracy of 83.85% on the test set. The ensemble fusion model based on a scoring mechanism achieved accuracy rates of 99.56%, 90.88%, and 87.97% on the training, validation, and test sets, respectively. The results indicated that the ensemble fusion model based on a scoring mechanism can enhance accuracy. Combining deep learning with NIR-HSI can effectively distinguish different varieties of watermelon seeds.

1. Introduction

The main uses of watermelon seeds are as seeds for planting and as edible kernels. As seeds, they can be planted to grow watermelons. Watermelon ranks among the key economic crops cultivated in 122 countries globally [1]. It is also a popular, delicious, and refreshing fruit, serving as a significant source of vitamins and minerals [2]. As food, they serve as a type of snack. Watermelon seeds represent a significant source of nutrients in the diet [3], and it may offer health and economic advantages owing to their fiber, mineral, phenolic content, and antioxidant activity. Therefore, it is very popular among everyone. The factors affecting watermelon quality include watermelon varieties, seed quality, environmental factors, and nutritional factors. Selecting suitable and high-quality seeds is particularly important [4]. In the actual market, the price of each watermelon seed varies, and they are often quite expensive. Due to the difficulty of distinguishing watermelon seeds by eyes, market transactions frequently encounter situations of substandard or adulterated seeds, causing harm to the interests of farmers. For watermelon seeds, the purity of the seeds (varieties) is crucial. Because impurities in seeds can cause unhealthy and uneven plant populations, leading to elevated production expenses and decreased yields [5]. With the increasing variety of watermelon seeds, there is an urgent need for a detection technology that can identify multiple varieties quickly and without causing damage.

Traditional approaches for seed variety detection encompass morphological methods [6], electrophoretic identification methods, fluorescence-based identification methods, and chemical identification methods, among others. However, these traditional detection approaches are time-consuming and labor-intensive and are not conducive to the efficient detection of smart agriculture. RGB cameras had been used for discriminating watermelon ploidy seeds [5]. When species have similar morphological features and colors, it is difficult to classify them using visual methods [7].

Machine vision only acquires image information within the visible light range. As the variety of seeds increases, their seed characteristics overlap severely, and a single technique cannot provide sufficient information for their classification. Hyperspectral imaging has the advantages of machine vision and visible infrared spectroscopy [8]. Near-infrared spectroscopy analysis technology had been widely applied in seed quality detection due to its inherent advantages [9]. It had been used for quality assessment in seeds such as wheat seeds [10, 11], peanut seeds [12], maize seeds [13], radish seeds [14], pine seeds [15], etc. However, traditional near-infrared spectroscopy analysis technology also had limitations. This technique could only analyze a single point on a seed and cannot comprehensively cover the entire seed. Therefore, for individual watermelon seeds, achieving the desired detection accuracy was challenging.

Near-infrared hyperspectral imaging (NIR-HSI) technology is a combination of imaging and spectroscopic detection techniques. Hyperspectral imaging captures spatial images of samples across various wavelengths in the electromagnetic spectrum, creating a three-dimensional hypercube. Due to the spectral and spatial information provided by hyperspectral imaging, it had gained popularity in various fields [16]. In hyperspectral image data, each band is a grayscale image and each pixel has a spectrum. Typically, the spectral average of the regions of interest in each band is utilized. NIR-HIS is an advanced technology engineered to swiftly and nondestructively assess the quality and safety of diverse agricultural products [17]. More and more scholars have been applying NIR-HSI technology to seed variety detection in recent years. In the field of watermelon varieties, Zhang et al. successfully classified watermelon seed varieties using BPNN and ELM models based on NIR-HIS [4]. Additionally, researchers had applied NIR-HSI to other seeds. Singh et al. successfully identified barley seed varieties by combining NIR-HSI with CNN [18]. Feng et al. used PCA-based SVM and RBFNN models to identify grape varieties in raisins [19]. Han et al. successfully classified licorice seeds by applying NIR-HSI combined with an SVM discriminant model based on feature bands [20]. Zhou et al. achieved the recognition of wheat grain varieties using a large near-infrared spectral dataset and a novel feature selection method based on deep learning [21]. In the field of cotton seed classification, a combination of NIR-HSI and partial least squares discriminant analysis (PLS-DA) were used to successfully classify variety [22].

Deep learning (DL) [23] stands as a pivotal artificial intelligence technique, empowering machines to autonomously glean knowledge from data. The application of DL is progressively expanding into the domain of spectral analysis [24]. Bai et al. utilized the combination of NIR-HSI and ResNet to achieve classification of coix seeds [25]. Barrio-Conde et al. utilized NIR-HSI combined with AlexNet to achieve classification of high oleic sunflower seed [26]. Previous studies had used a single model. This study would use multiple models to integrate to improve the learning ability of features. The studies mentioned above all used a single network architecture and a single-scale feature extraction capability. When encountering more complex problems, the accuracy of a single network may be limited. In practice, near-infrared hyperspectral data exhibited characteristics such as large data volume, high noise, and high dimensionality. Therefore, there would be a considerable amount of redundant information in the modeling process, posing challenges for model classification. Typical techniques for dimensionality reduction encompass principal component analysis (PCA), successive projections algorithm (SPA), and various other approaches. In recent years, some scholars have employed a combination of PCA and SPA dimensionality reduction algorithms with hyperspectral imaging systems to classify three different degrees of freeze damage in corn seeds [27]. Soybean classification had been achieved using PCA and artificial neural network (ANN) classifiers [28]. The construction of spectral feature vectors using SPA had been applied to the classification of waxy corn seed varieties [7]. The SPA had been utilized to select the optimal wavelength for corn seed variety classification [29]. In summary, combining hyperspectral data with deep learning models for dimensionality reduction and accuracy improvement is very meaningful.

Maintaining variety purity is crucial throughout the agricultural process due to its significant benefits for seed storage and economic efficiency [30]. This study explored a model suitable for classifying 10 watermelon varieties. Additionally, confusion matrices were utilized for visualizing prediction results, and a weighted scoring mechanism was employed to improve the accuracy of the deep learning models. The primary objectives of this study are (1) to classify 10 watermelon seed varieties using NIR-HSI technology combined with deep learning models; (2) to explore the enhancement of model accuracy through a weighted scoring mechanism; (3) to explore the optimal combination of initial points and the number of bands in the SPA.

2. Materials and Methods

2.1. Material Preparation and Data Division. There were 10 kinds of watermelon varieties, respectively, Quanmei2k, Quanmei4k, Quanmei8k, Xinxin, Caihongguazhibao, Heishuai, Mingyu, Zaojia, Yuyiguazhibaojiuhao, and Yuyijinxiabahao (Figure 1). A total of 2283 watermelon seed samples were used in this study. The detailed distribution of samples is shown in Table 1. The dataset was divided in a 6 : 1 : 1 ratio. The watermelon seeds used in this study were provided by Zhejiang Provincial Seed Management Station.

2.2. Acquisition and Correction of Near-Infrared Hyperspectral Images. The hyperspectral imaging platform (Specim, Spectral Imaging Ltd., Oulu, Finland) used in this study belongs to the LSCA-0720-148 series. The scanning speed of the equipment was set at 24.7 mm/s, with a frame rate of 70 Hz. Due to the influence of dark current, white reference images and dark reference images should be used to correct the acquired raw hyperspectral images to reflective hyperspectral images. A white reference board was placed in

Table 1: Dataset partitioning of watermelon seeds.

Variety	Training	Validation	Test	Total
Caihongguazhibao	87	14	15	116
Heishuai	226	38	38	302
Mingyu	226	38	38	302
Quanmei2k	150	25	26	201
Quanmei4k	152	25	26	203
Quanmei8k	147	25	25	197
Xinxin	258	43	44	345
Yuyijinxiabahao	85	14	15	114
Yuyiguazhibaojiuhao	96	16	17	129
Zaojia	280	47	47	374
Total	1707	285	291	2283

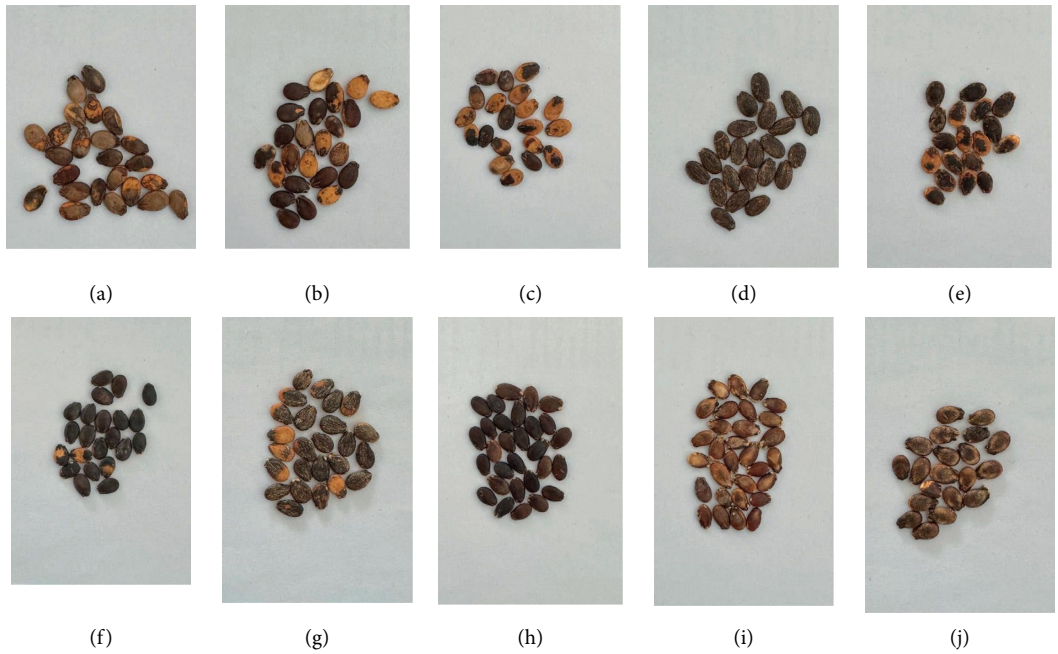

Figure 1: Watermelon seed images. (a) Zaojia. (b) Caihongguazhibao. (c) Yuyiguazhibaojiuhao. (d) Yuyijinxiabahao. (e) Heishuai. (f) Mingyu. (g) Xinxin. (h) Quanmei2k. (i) Quanmei4k. (j) Quanmei8k.

front of the object to obtain a white reference image for light intensity calibration, while a dark reference image was obtained using a black opaque lens cover for dark current removal. The corrected image can be obtained by the formula as follows:

$$R = \frac{I - D}{W - D}, \tag{1}$$

where I represents the original image, R is the corrected image, W denotes the white reference image, and D is the dark reference image.

Due to the presence of noise before and after the bands, and the 1140–1350 nm wavelength range being utilized for detecting the C-H second overtone [6], this study adopted a wavelength range of 1053.43 to 1680.87 nm. In this research, every seed within the hyperspectral image was regarded as a region of interest (ROI), where the spectrum of each pixel within the ROI was averaged to derive a spectral vector representing the seed sample.

2.3. Spectral Preprocess. The spectral reflectance data obtained from the experiments were coarse and contained noise caused by factors such as equipment, experimental environment, and sample impurities. To reduce the impact of noise on the results, the Savitzky–Golay (SG) smoothing algorithm and the standard normal variate (SNV) algorithm were employed in this study. The working principle of the SG smoothing algorithm [31] is to slide a window over the data and, at each position, fit a polynomial to the points within the window. The center point of the window is replaced by the value estimated by the polynomial fit. This process is repeated for each point in the data, effectively smoothing and reducing noise. In this study, the SG cubic polynomial 7-point smoothing method was used to process the spectral data. The SNV (formula (2)) centralized and standardized the spectral data, making the mean of the data equal to 0 and the variance equal to 1. The use of SNV could effectively eliminate unwanted variations, such as baseline shifts and drifts [32]. SNV could enhance the stability and reliability of

spectral data, improving data comparability and interpretability. The successive projections algorithm (SPA) is a commonly used method for selecting feature wavelengths [33]. SPA is a variable selection algorithm designed to choose wavelengths with minimal redundant information [34]. Therefore, SPA was selected as the wavelength selection algorithm.

$$x_{\mathrm{SNV}} = \frac{x - \overline{x}}{\sqrt{\left(\sum_{k=1}^{m} (x_k - \overline{x})^2 / (m-1)\right)}}, \tag{2}$$

where $\overline{x} = \sum_{k=1}^{m} x_k / m$, m is the number of bands, and $k = 1, 2, 3, \ldots, m$.

2.4. Classification Model and Scoring Mechanism

2.4.1. XGBoost and SVM. The extreme gradient boosting (XGBoost) model is currently the fastest and most effective ensemble decision tree algorithm and has been successfully applied in many fields [35]. He et al. utilized hyperspectral imaging (HSI) technology combined with the XGBoost model to accurately differentiate between naturally ripened and artificially ripened bananas [36]. Support vector machine (SVM) is one of the most efficient supervised classification methods [37]. The combination of HSI technology and support vector machine (SVM) has been widely used in various applications such as variety identification [25]. Zhang et al. utilized traditional machine learning and deep learning to identify different levels of freezing damage in corn seeds [38]. The results showed that deep learning performed the best.

2.4.2. LeNet Model. The LeNet model stood out as one of the pioneering convolutional neural networks [39]. In its architectural composition, the LeNet model comprised two integral components: a convolutional encoder and a densely connected block. The LeNet structure implemented in this study encompassed 3 convolutional layers, 3 max-pooling layers, 3 activation functions, 3 batch normalization layers, and 1 fully connected layer (Figure 2(a)). The convolutional layers utilized 1×4 convolutional kernels with channel numbers 8, 16, and 32. Feature extraction was facilitated through max-pooling layers with a kernel size of 1×4 and a stride of 1. The ReLU function was employed as the activation function.

2.4.3. GoogLeNet Model. Inception was a deep convolutional neural network architecture [40]. The Inception module can obtain information at multiple scales. The main characteristic of this architecture was the improvement of internal computational resource utilization within the network. While focusing on deepening the network structure, GoogLeNet introduced a new fundamental structure called the Inception module to increase the network's width. The Inception module in the GoogLeNet model utilized different convolutional kernels to extract information at various levels, employed 1×1 convolutional kernels for dimension reduction and computational efficiency, increased the model depth, and enhanced nonlinear expression capability. The GoogLeNet model (Figure 2(b)) employed in this study consists of two convolutional layers, two Inception modules, 2 max-pooling layers, 2 activation functions, 2 batch normalization layers, and 1 fully connected layer. The convolutional layers had kernels of size 1×5 with channel numbers of 10 and 20, respectively. The Inception module (Figure 2(d)) consists of four parallel pathways. Different paths can obtain different feature information, which is more conducive to model analysis. Finally, all four paths used appropriate padding to ensure consistency in height and width between input and output.

2.4.4. ResNet Model. He et al. introduced the residual learning framework (ResNet) to simplify the training of deeper networks compared to previous approaches [41]. ResNet had become the most cited neural network of the 21st century.

For a stacked-layer structure (composed of several stacked layers), when the input is x and the learned features are denoted as $H(x)$, the goal is to learn the residual $F(x) = H(x) - x$. This means that the original learned features are essentially $F(x) + x$. The reason for using this approach is that learning the residual is easier compared to directly learning the original features. When the residual is 0, the stacked layers essentially perform an identity mapping, ensuring that the network's performance does not degrade. In practice, the residual is not exactly 0, allowing the stacked layers to learn new features on top of the input features, leading to improved performance. The structure of the ResNet model in this study is depicted in Figure 2(c). The ResNet model employed in this study consisted of two convolutional layers, two residual modules, 2 max-pooling layers, 2 activation functions, 2 batch normalization layers, and 1 fully connected layer. The convolutional layers had kernels of size 1×5 with channel numbers of 16 and 32, respectively. The residual module is shown in Figure 2(e). The residual module directly transmits feature information through a short-circuit-like connection method.

2.4.5. Scoring Mechanism Model. Ensemble learning was a method that helps improve the predictive accuracy of machine learning [42]. The objective of ensemble methods was to amalgamate various classifiers into a metaclassifier possessing superior generalization capabilities when compared to individual classifiers within it.

The approach studied in this study was the multimodel weighted scoring model. It combined the predicted results of models through a series of weighted summations. It selected the highest score for output and thereby improved overall accuracy. In the first step, the output values of each model were transformed using the formula (3), ensuring nonnegativity of the output. In the second step, the weighted formula (formula (4)) was employed to output the highest score. The workflow diagram of the score-based ensemble fusion model in this study is shown in Figure 3.

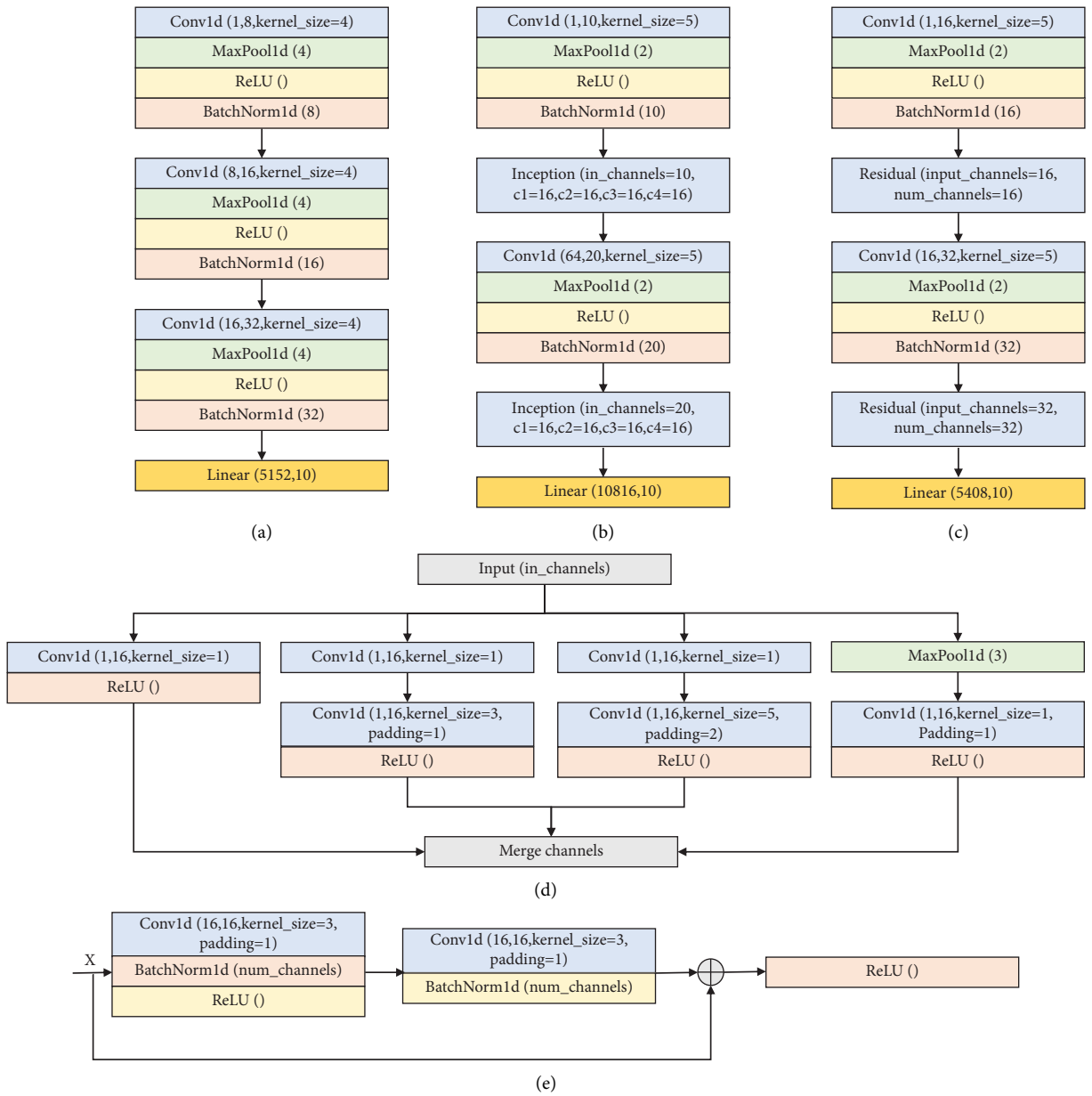

Figure 2: Structure of models: (a) LeNet structure; (b) GoogLeNet structure; (c) ResNet structure; (d) inception of GoogLeNet; (e) residual of ResNet.

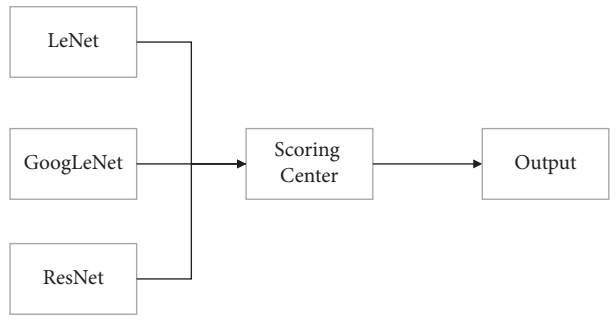

Figure 3: Scoring mechanism model.

$$y_j = \frac{\exp(o_j)}{\sum_k \exp\ (o_k)}, \tag{3}$$

where o_j represents the output value indicating the classification as the j-th category and y_j represents the output value indicating the classification as the j-th category after nonnegative transformation.

$$y\_\text{hat} = \sum_{i=1}^{n} a_i \times y\_\text{hat}_i, \tag{4}$$

where y_hat represents the prediction result of the ensemble model, a_i represents the weight coefficient corresponding to each model, and y_hat$_i$ represents the prediction result of each model.

2.5. Model Evaluation and Implementation Details. Figure 4 represents the schematic structure of the entire experiment. The evaluation of model performance in this study employed the classification accuracy metric. Classification accuracy is defined as the ratio of correct predictions to the total number of predictions made. Deep learning models were built using the PyTorch (version 1.12.1) framework. Data analyses were carried out on a computer equipped with an NVIDIA GeForce RTX 4060 Laptop GPU.

3. Results and Discussion

3.1. Spectral Analysis. The spectral feature of each seed was derived by computing the average value of all pixels within the corresponding region of interest (ROI) across effective bands. Figure 5(a) shows the original spectral data of watermelon seeds, revealing discrete data that were not conducive to data analysis. Therefore, it could apply Savitzky–Golay (SG) and standard normal variate (SNV) for denoising (Figure 5(b)). Figure 5(c) shows the average spectra for each watermelon seed variety. Differences were noted in the average spectra across various types of watermelon seed varieties. The average spectrum of Mingyu differed significantly from the other nine varieties. As different watermelon seeds contained varying chemical components such as proteins, the wavelength range of 1140–1350 nm was utilized for detecting the C-H second overtone [6]. Distinct disparities were noted in the average spectra of different watermelon varieties within the range of 1100–1300 nm (Figure 5(c)). In the remaining wavelength ranges, differences between some varieties were less pronounced. Overall, there were variations in the average spectra of samples from different watermelon varieties, indicating the feasibility of classifying watermelon seed varieties.

3.2. Dimensionality Reduction Results' Analysis

3.2.1. Loss Values in Different Band Numbers. Figure 6 shows the values of the loss function on the validation sets for various models under different numbers of spectral bands. Figure 6(a) shows loss function values of LeNet. Figure 6(b) shows loss function of GoogLeNet. Figure 6(c) shows loss function of ResNet. While computing the loss function, the model's hyperparameters remain consistent, with only the number of spectral bands varying. The cross-entropy loss function was used as the loss function. This study defined effective dimensionality reduction as reducing the number of bands to within 100 dimensions. In the models, lower loss function values indicated a closer proximity to the true classification results. The loss function values for all three models were decreasing, primarily due to the increase in spectral information. Around 80–100 bands, the loss function values for all three models were stabilized. It indicated that the added spectral information no longer significantly contributes to the differentiation of the classification models (Figure 6).

3.2.2. Specific Bands. Table 2 shows the wavelength ranges corresponding to the input features for each best model after dimensionality reduction. Due to variations in chemical components such as proteins among different watermelon seeds, the wavelength range of 1140–1350 nm was essential for detecting the second overtone of C-H bonds [6]. In this research, the initial point selected by the successive projections algorithm (SPA) was the 26th band at a wavelength of 1140.47 nm. As the loss values decrease, the band range essentially covered 1140–1350 nm. The LeNet model took 90 bands determined by SPA as input, the GoogLeNet model took 90 bands determined by SPA as input, and the ResNet model took 87 bands determined by SPA as input. The determination of the number of bands for each model was based on extensive experimentation (Figure 6). The selection aimed to achieve maximum dimensionality reduction while maintaining accuracy.

3.3. Classification Results' Analysis

3.3.1. Confusion Matrix Results. Figure 7 displays the confusion matrices illustrating the classification results of the three best deep learning models on the validation set. Figure 7(d) shows the variety label. This matrix facilitated the observation of correct predictions and misclassifications for each category. The visualization of model prediction results through confusion matrices is beneficial for the analysis of scoring mechanisms. In Figure 7(a), it could be observed that the LeNet model was prone to misclassify Quanmei8k as Zaojia, Xinxin as Zaojia, and Zaojia as Xinxin. In Figure 7(b), the GoogLeNet model tended to misclassify Quanmei8k as Zaojia and Zaojia tended to be misclassified as Quanmei8k. In Figure 7(c), the ResNet model tended to misclassify Quanmei8k as Quanmei4k and Xinxin as Quanmei4k. By observing the confusion matrix, this study found that different models exhibited inconsistent accurate classification results for different seed varieties. There were cases where two models had accurate classifications, but another model had misclassifications. Therefore, this study proposed a scoring mechanism model to enhance accuracy.

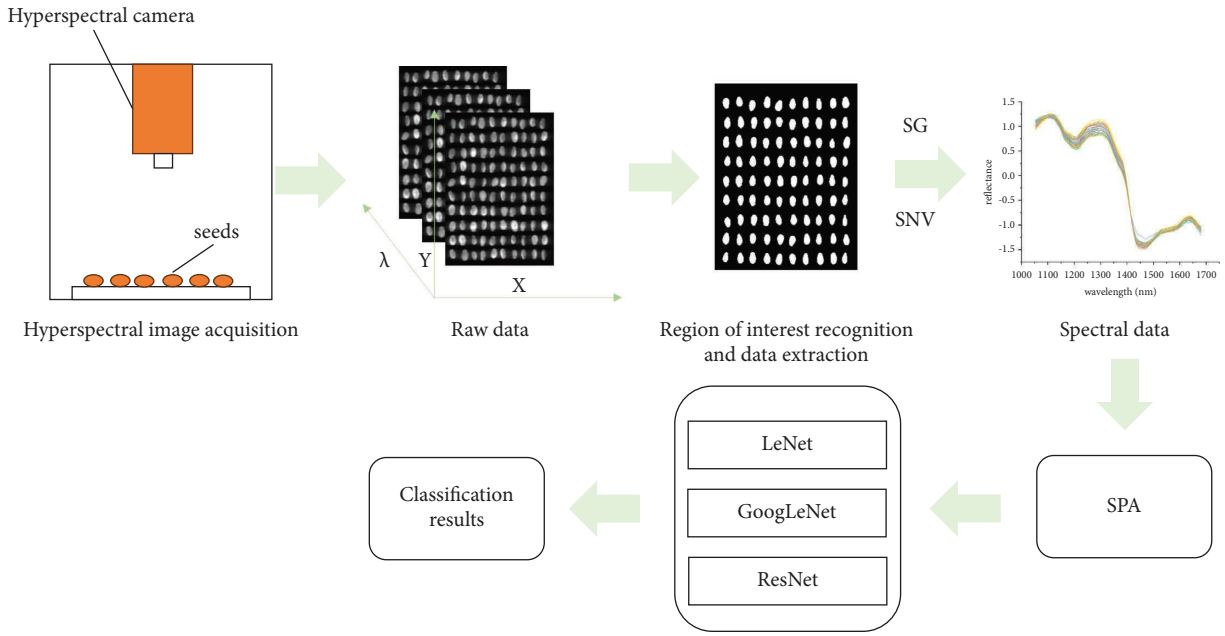

Figure 4: The steps of the proposed method (first, near-infrared hyperspectral images' acquisition and preprocessing were performed. The successive projections algorithm was used for data dimensionality reduction. Models (LeNet, GoogLeNet, and ResNet) were performed to classify. Finally, three models were integrated by a scoring mechanism).

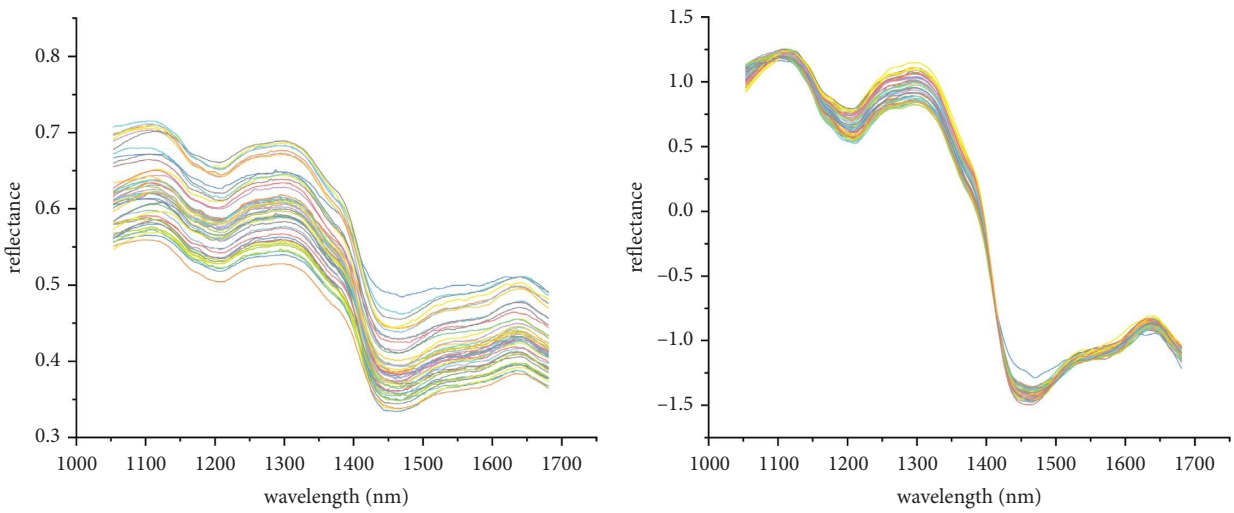

Figure 5: Continued.

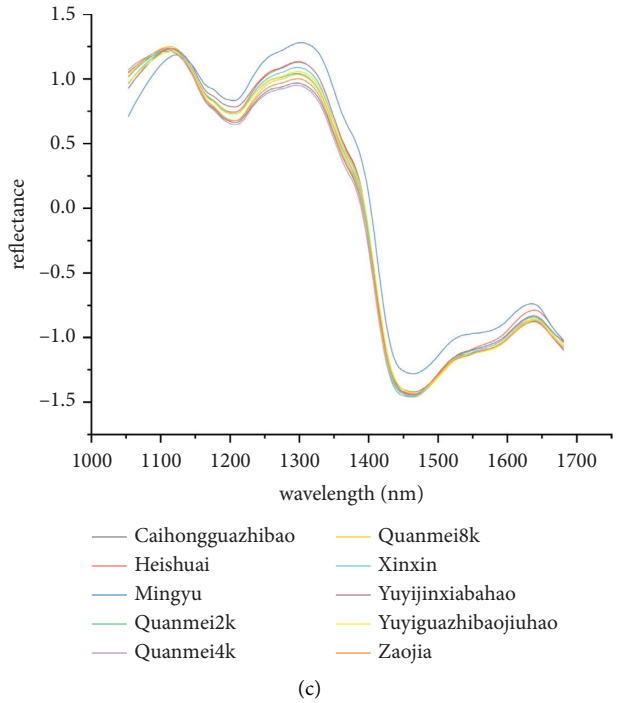

(c)

Figure 5: Spectral data: (a) raw spectral data; (b) data after SG and SNV; (c) average spectrum of different watermelon seeds.

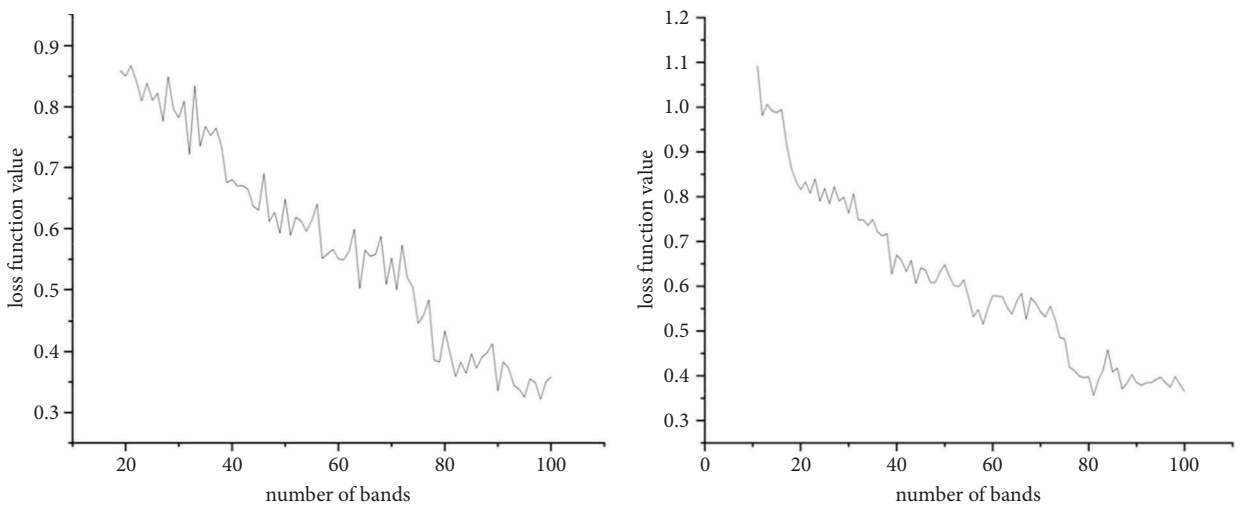

(a) (b)

Figure 6: Continued.

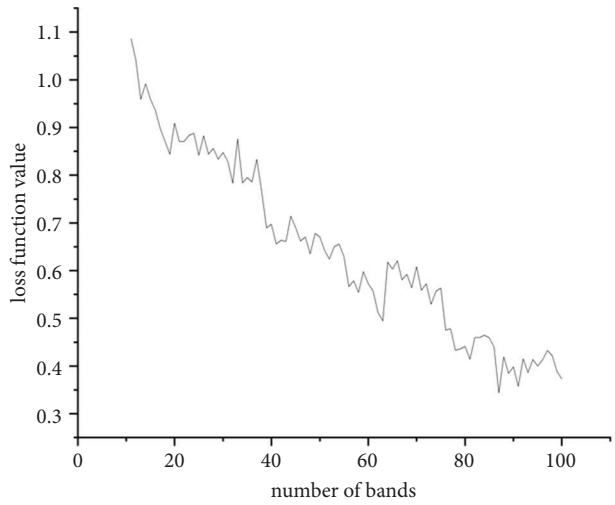

(c)

Figure 6: Loss values of models: (a) loss values of LeNet; (b) loss values of GoogLeNet; (c) loss values of ResNet.

Table 2: Model specific bands.

Model	Wavelength (nm)
LeNet	1053.43, 1056.9, 1060.38, 1063.85, 1067.33, 1070.81, 1074.29, 1077.76, 1081.24, 1140.47, 1203.37, 1206.87, 1210.37, 1213.87, 1217.37, 1269.95, 1273.46, 1276.97, 1280.48, 1283.99, 1287.51, 1291.02, 1294.53, 1298.05, 1301.56, 1305.08, 1308.59, 1312.11, 1315.62, 1319.14, 1322.66, 1326.18, 1329.7, 1333.22, 1336.74, 1340.26, 1343.78, 1396.67, 1400.2, 1403.73, 1407.26, 1410.79, 1414.32, 1417.86, 1421.39, 1424.92, 1428.46, 1531.21, 1534.76, 1538.32, 1541.87, 1545.42, 1548.98, 1552.53, 1556.09, 1559.64, 1563.2, 1566.75, 1570.31, 1573.87, 1577.43, 1580.99, 1584.55, 1588.11, 1591.67, 1595.23, 1598.79, 1602.35, 1605.92, 1609.48, 1613.04, 1616.61, 1620.17, 1623.74, 1627.31, 1630.87, 1634.44, 1638.01, 1641.58, 1645.15, 1648.71, 1652.29, 1655.86, 1659.43, 1663, 1666.57, 1670.14, 1673.72, 1677.29, 1680.87
GoogLeNet	1053.43, 1056.9, 1060.38, 1063.85, 1067.33, 1070.81, 1074.29, 1077.76, 1081.24, 1140.47, 1203.37, 1206.87, 1210.37, 1213.87, 1217.37, 1269.95, 1273.46, 1276.97, 1280.48, 1283.99, 1287.51, 1291.02, 1294.53, 1298.05, 1301.56, 1305.08, 1308.59, 1312.11, 1315.62, 1319.14, 1322.66, 1326.18, 1329.7, 1333.22, 1336.74, 1340.26, 1343.78, 1396.67, 1400.2, 1403.73, 1407.26, 1410.79, 1414.32, 1417.86, 1421.39, 1424.92, 1428.46, 1531.21, 1534.76, 1538.32, 1541.87, 1545.42, 1548.98, 1552.53, 1556.09, 1559.64, 1563.2, 1566.75, 1570.31, 1573.87, 1577.43, 1580.99, 1584.55, 1588.11, 1591.67, 1595.23, 1598.79, 1602.35, 1605.92, 1609.48, 1613.04, 1616.61, 1620.17, 1623.74, 1627.31, 1630.87, 1634.44, 1638.01, 1641.58, 1645.15, 1648.71, 1652.29, 1655.86, 1659.43, 1663, 1666.57, 1670.14, 1673.72, 1677.29, 1680.87
ResNet	1053.43, 1056.9, 1060.38, 1063.85, 1067.33, 1070.81, 1074.29, 1077.76, 1081.24, 1140.47, 1206.87, 1210.37, 1213.87, 1217.37, 1269.95, 1273.46, 1276.97, 1280.48, 1283.99, 1287.51, 1291.02, 1294.53, 1298.05, 1301.56, 1305.08, 1308.59, 1312.11, 1315.62, 1319.14, 1322.66, 1326.18, 1329.7, 1333.22, 1336.74, 1340.26, 1343.78, 1396.67, 1400.2, 1403.73, 1407.26, 1410.79, 1414.32, 1417.86, 1421.39, 1424.92, 1428.46, 1538.32, 1541.87, 1545.42, 1548.98, 1552.53, 1556.09, 1559.64, 1563.2, 1566.75, 1570.31, 1573.87, 1577.43, 1580.99, 1584.55, 1588.11, 1591.67, 1595.23, 1598.79, 1602.35, 1605.92, 1609.48, 1613.04, 1616.61, 1620.17, 1623.74, 1627.31, 1630.87, 1634.44, 1638.01, 1641.58, 1645.15, 1648.71, 1652.29, 1655.86, 1659.43, 1663, 1666.57, 1670.14, 1673.72, 1677.29, 1680.87

3.3.2. Model Classification Results. Table 3 displays the average accuracy and variance of each model. The results indicated that the classification performance of traditional machine learning (XGBoost, SVM) was not as good as that of deep learning models. The reason may be that deep learning had a stronger feature representation ability. Deep learning can typically automatically extract features through end-to-end learning, giving it an advantage in feature representation. Deep learning models usually have stronger generalization ability, enabling them to better adapt to new

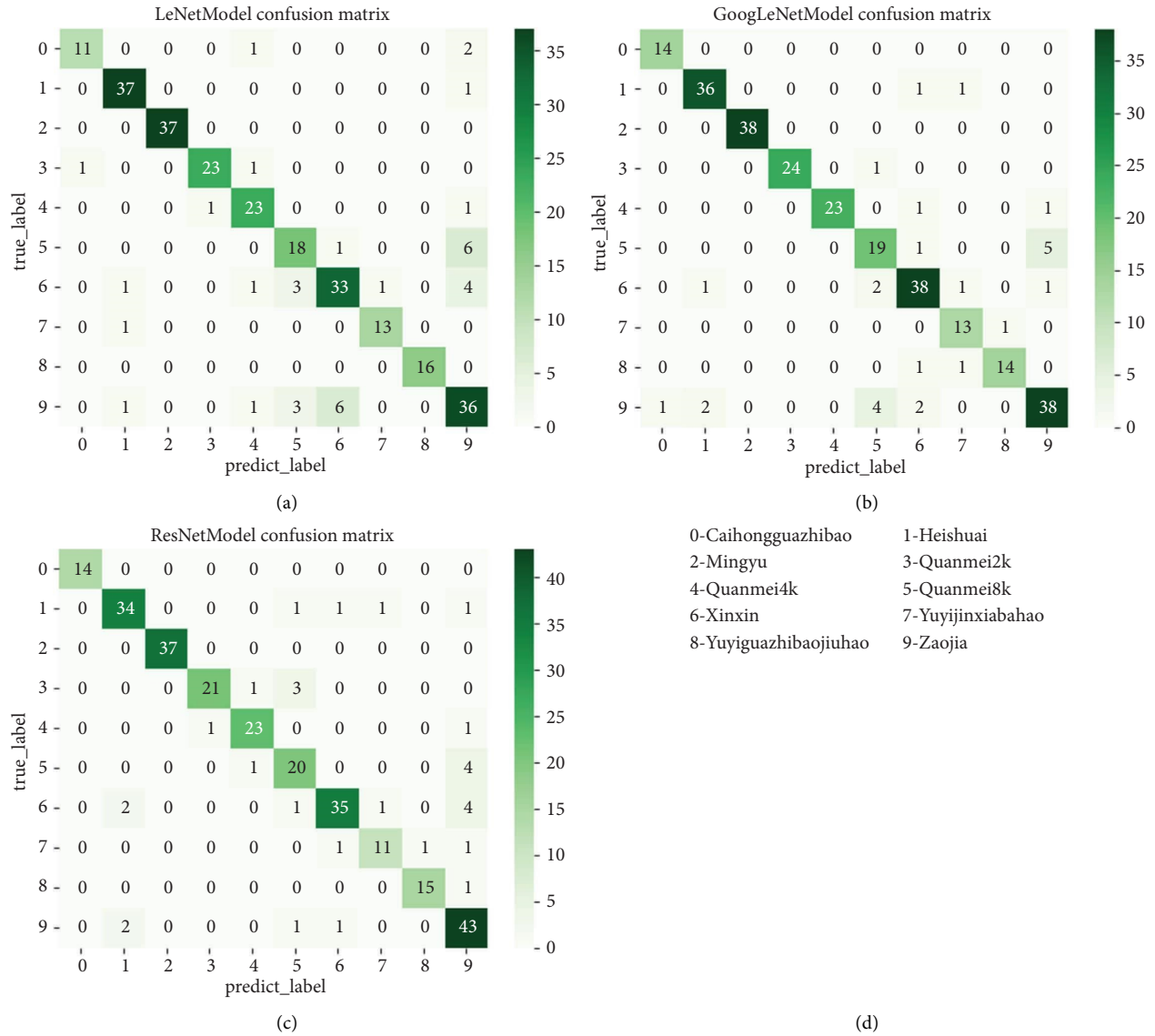

Figure 7: Confusion matrices of models (a) LeNetModel confusion matrix; (b) GoogLeNetModel confusion matrix; (c) ResNetModel confusion matrix; (d) variety label.

Table 3: Model classification results.

Model	Training (%)		Validation (%)		Test (%)	
	Accuracy	s^2	Accuracy	s^2	Accuracy	s^2
XGBoost	88.49	0.04	62.64	0.28	65.46	3.57
SVM	92.94	0.00*	79.58	0.28	78.01	0.12
LeNet	97.28	0.82	87.20	0.03	85.22	1.06
GoogLeNet	98.42	0.01	89.65	0.28	84.71	0.27
ResNet	99.94	0.00*	88.60	0.28	86.77	0.27
Scoring mechanism model	99.56	0.00*	90.88	4.43	87.97	2.96
XGBoost + SPA	85.15	0.62	61.58	0.28	67.01	26.25
SVM + SPA	85.18	0.01	79.13	0.77	77.15	1.44
LeNet + SPA†	90.89	0.01	88.78	6.03	83.51	1.89
GoogLeNet + SPA†	91.74	0.58	86.32	0.50	83.85	1.89
ResNet + SPA†	93.03	16.81	85.24	1.70	82.99	1.44
Scoring mechanism model + SPA†	93.94	3.40	90.00	6.92	84.71	2.39

†: SPA is the successive projections algorithm. *: it is approximately equal to zero after rounding, and s^2: s^2 is variance.

data and unseen situations. On the test set, the scoring mechanism model has a higher average accuracy than the other models, but its variance is higher compared to the other models. In the full band, the ResNet model showed the best classification performance, achieving an accuracy of 86.77% on the test set. By using characteristic bands, the GoogLeNet model performed best, with a classification accuracy of 83.85% on the test set. In the full band, the model based on the scoring mechanism achieved accuracies of 99.56%, 90.88%, and 87.97% on the training, validation, and test sets, respectively. By using characteristic bands, the scoring mechanism model achieved accuracies of 93.94%, 90.00%, and 84.71% on the training, validation, and test sets, respectively (Table 3). The scoring mechanism model scoring mechanism showed an improvement in accuracy compared to single models. This improvement was attributed to the enhanced generalization of the models through the scoring mechanism, leading to higher accuracy. After applying the successive projections algorithm (SPA), the LeNet model used 90 bands from the SPA result, the GoogLeNet model used 90 bands from the SPA result, and the ResNet model used 87 bands from the SPA result (Table 2). The initial band was selected at the wavelength of 1140.47 nm. It could achieve not only dimensionality reduction but also demonstrate a relatively good classification performance. Compared to models without using the successive projections algorithm, there was a slight decrease in accuracy. This decrease was due to the reduction in data dimensions, leading to information loss. However, utilizing SPA resulted in a reduction in data complexity and an improvement in computational speed.

3.4. Discussion. The identification of watermelon varieties was highly significant for reducing the adulteration of watermelon seeds and minimizing losses for farmers. In this study, near-infrared hyperspectral imaging technology was employed for watermelon seed variety classification. In summary, the scoring mechanism model achieved the best results in terms of accuracy, indicating the superiority of the scoring mechanism model. It was an effective approach. The integration of ensemble techniques enhanced the model's generalization ability, subsequently improving accuracy. Within this study, the successive projections algorithm (SPA) was utilized for data dimensionality reduction, resulting in an enhanced computational speed. However, by using SPA, the accuracy of models decreased. The main reason for that was the decrease in data information. Based on the overall results, the model constructed in this study may exhibit signs of overfitting. We believe that the primary reason for this may be the insufficient coverage of the entire data distribution by the training data, leading to the model's inability to generalize well to new data. In the future, we propose collecting more diverse and abundant watermelon seed data or using techniques like generative adversarial networks (GANs) to generate more varied data. This aims to enhance the model's adaptability to different scenarios and variations. From the perspective of parameter quantity, integrating multiple models into an ensemble model resulted in a higher number of parameters compared to a single model, leading to increased computational workload during model computation. From the perspective of accuracy, ensemble models had the ability to capture features at different scales and demonstrated improved accuracy. In previous studies on watermelon variety classification using near-infrared spectroscopy (NIR), Deák et al. utilized a more traditional qualitative evaluation polar qualification system (PQS) with automatic wavelength range optimization for analysis [43]. Near-infrared hyperspectral imaging (NIR-HSI) combines the advantages of machine vision and near-infrared spectroscopy. Although NIR spectroscopy technology is cheaper than NIR-HSI, the data information obtained is limited. Compared to NIR spectroscopy, NIR-HSI technology can capture the entire seed's spectral information. It makes the analysis results more accurate. In the future, NIR-HSI technology can be applied to the detection of watermelon vitality. Compared to the study by Mukasa et al. [5], we successfully classified 10 watermelon seed varieties, achieving good classification results. Compared to the watermelon variety classification by Zhang et al. [4], this study utilized the popular convolutional neural network (CNN) for modeling. Compared to previous studies that combined NIR-HSI with DL [25], this study integrated a single network using a scoring mechanism, further improving the effectiveness. The sample size in this study was relatively limited and may be expanded in future research. For our model, transferring this model and research results to new varieties is a challenging task. At present, we believe that transfer learning and incremental learning may help address this issue.

4. Conclusion

In the research, a near-infrared hyperspectral imaging technology system and deep learning were successfully applied to the classification of watermelon seeds. Experimental results suggested that the best deep learning models to classify watermelon seeds was the ResNet model with a model accuracy of 86.77% on the test set. In contrast to prior research, this study facilitated the enhanced utilization of deep learning models in seed classification, resulting in improved efficiency. For this purpose, the scoring mechanism was used for the integration of three deep learning models, and the accuracy of the scoring mechanism model on the test set is 87.97%. In addition, the accuracy of deep learning models using the SPA was lower than that of models using full spectra on the test set. For future exploration, the study will delve into classifying a broader range of watermelon seed varieties. The watermelon seed classification model was used as the foundation for the classification of other seeds to save the time of model training by transfer learning.

Data Availability

The data used to support the findings of this study will be made available upon reasonable request from the corresponding author.

Conflicts of Interest

The authors declare that they have no conflicts of interest.

Authors' Contributions

Hengnian Qi handled software, carried out methodology, and collected resources; Mengbo He handled software and carried out methodology and writing of the original draft; Zihong Huang collected resources and performed data curation; Jianfang Yan collected resources and conducted investigation. Chu Zhang was involved in conceptualization, methodology, and software. The authors Hengnian Qi and Mengbo He contributed equally to this manuscript.

Acknowledgments

This work was funded by the Zhejiang Key R&D Plan (2019C02013).

References

[1] J. Yasmin, M. R. Ahmed, C. Wakholi et al., "Near-infrared hyperspectral imaging for online measurement of the viability detection of naturally aged watermelon seeds," *Frontiers in Plant Science*, vol. 13, Article ID 986754, 2022.

[2] M. R. Ahmed, J. Yasmin, E. Park et al., "Classification of watermelon seeds using morphological patterns of X-ray imaging: a comparison of conventional machine learning and deep learning," *Sensors*, vol. 20, no. 23, p. 6753, 2020.

[3] B. Tabiri, J. K. Agbenorhevi, F. D. Wireko-Manu, and E. I. Ompouma, "Watermelon seeds as food: nutrient composition, phytochemicals and antioxidant activity," *International Journal of Nutrition and Food Sciences*, vol. 5, no. 2, p. 139, 2016.

[4] C. Zhang, F. Liu, W. Kong, H. Zhang, and Y. He, "Fast identification of watermelon seed variety using near infrared hyperspectral imaging technology," *Transactions of the Chinese Society of Agricultural Engineering*, vol. 29, no. 20, pp. 270–277, 2013, https://www.ingentaconnect.com/content/tcsae/tcsae/2013/00000029/00000020/art00035?crawler=true&mimetype=application/pdf.

[5] P. Mukasa, C. Wakholi, M. Akbar Faqeerzada et al., "Non-destructive discrimination of seedless from seeded watermelon seeds by using multivariate and deep learning image analysis," *Computers and Electronics in Agriculture*, vol. 194, Article ID 106799, 2022.

[6] B. Jin, C. Zhang, L. Jia et al., "Identification of rice seed varieties based on near-infrared hyperspectral imaging technology combined with deep learning," *ACS Omega*, vol. 7, no. 6, pp. 4735–4749, 2022.

[7] X. Yang, H. Hong, Z. You, and F. Cheng, "Spectral and image integrated analysis of hyperspectral data for waxy corn seed variety classification," *Sensors*, vol. 15, no. 7, pp. 15578–15594, 2015.

[8] C. Xia, S. Yang, M. Huang, Q. Zhu, Y. Guo, and J. Qin, "Maize seed classification using hyperspectral image coupled with multi-linear discriminant analysis," *Infrared Physics and Technology*, vol. 103, Article ID 103077, 2019.

[9] Z. Wang, S. Fan, J. Wu et al., "Application of long-wave near infrared hyperspectral imaging for determination of moisture content of single maize seed," *Spectrochimica Acta Part A: Molecular and Biomolecular Spectroscopy*, vol. 254, Article ID 119666, 2021.

[10] S. R. Delwiche, "Protein content of single kernels of wheat by near-infrared reflectance spectroscopy," *Journal of Cereal Science*, vol. 27, no. 3, pp. 241–254, 1998.

[11] J. P. Nielsen, D. K. Pedersen, and L. Munck, "Development of nondestructive screening methods for single kernel characterization of wheat," *Cereal Chemistry*, vol. 80, no. 3, pp. 274–280, 2003.

[12] B. L. Tillman, D. W. Gorbet, and G. Person, "Predicting oleic and linoleic acid content of single peanut seeds using near-infrared reflectance spectroscopy," *Crop Science*, vol. 46, no. 5, pp. 2121–2126, 2006.

[13] J. G. Tallada, N. Palacios-Rojas, and P. R. Armstrong, "Prediction of maize seed attributes using a rapid single kernel near infrared instrument," *Journal of Cereal Science*, vol. 50, no. 3, pp. 381–387, 2009.

[14] N. Shetty, T. G. Min, R. Gislum, M. H. Olesen, and B. Boelt, "Optimal sample size for predicting viability of cabbage and radish seeds based on near infrared spectra of single seeds," *Journal of Near Infrared Spectroscopy*, vol. 19, no. 6, pp. 451–461, 2011, https://opg.optica.org/jnirs/abstract.cfm?uri=jnirs-19-6-451.

[15] M. Tigabu, A. Daneshvar, R. Jingjing, P. Wu, X. Ma, and P. C. Odén, "Multivariate discriminant analysis of single seed near infrared spectra for sorting dead-filled and viable seeds of three pine species: does one model fit all species?" *Forests*, vol. 10, no. 6, p. 469, 2019.

[16] W. Kong, C. Zhang, F. Liu, P. Nie, and Y. He, "Rice seed cultivar identification using near-infrared hyperspectral imaging and multivariate data analysis," *Sensors*, vol. 13, no. 7, pp. 8916–8927, 2013.

[17] D. Khamsopha, S. Woranitta, and S. Teerachaichayut, "Utilizing near infrared hyperspectral imaging for quantitatively predicting adulteration in tapioca starch," *Food Control*, vol. 123, Article ID 107781, 2021.

[18] T. Singh, N. M. Garg, and S. R. Iyengar, "Nondestructive identification of barley seeds variety using near-infrared hyperspectral imaging coupled with convolutional neural network," *Journal of Food Process Engineering*, vol. 44, no. 10, Article ID 13821, 2021.

[19] L. Feng, S. Zhu, C. Zhang, Y. Bao, P. Gao, and Y. He, "Variety identification of raisins using near-infrared hyperspectral imaging," *Molecules*, vol. 23, no. 11, p. 2907, 2018.

[20] Q. Han, Y. Li, and L. Yu, "Classification of glycyrrhiza seeds by near infrared hyperspectral imaging technology," in *2019 International Conference on High Performance Big Data and Intelligent Systems (HPBD&IS)*, pp. 141–145, IEEE, Piscataway, NJ, United States, 2019.

[21] L. Zhou, C. Zhang, M. F. Taha et al., "Wheat kernel variety identification based on a large near-infrared spectral dataset and a novel deep learning-based feature selection method," *Frontiers in Plant Science*, vol. 11, Article ID 575810, 2020.

[22] S. F. Carreiro Soares, E. P. Medeiros, C. Pasquini, C. de Lelis Morello, R. K. Harrop Galvão, and M. C. Ugulino Araújo, "Classification of individual cotton seeds with respect to variety using near-infrared hyperspectral imaging," *Analytical Methods*, vol. 8, no. 48, pp. 8498–8505, 2016, https://pubs.rsc.org/en/content/articlelanding/2016/ay/c6ay02896a/unauth.

[23] M. I. Jordan and T. M. Mitchell, "Machine learning: trends, perspectives, and prospects," *Science*, vol. 349, no. 6245, pp. 255–260, 2015.

[24] X. Jin, L. Jie, S. Wang, H. J. Qi, and S. W. Li, "Classifying wheat hyperspectral pixels of healthy heads and Fusarium head blight disease using a deep neural network in the wild field," *Remote Sensing*, vol. 10, no. 3, p. 395, 2018.

[25] R. Bai, J. Zhou, S. Wang et al., "Identification and classification of Coix seed storage years based on hyperspectral imaging technology combined with deep learning," *Foods*, vol. 13, no. 3, p. 498, 2024.

[26] M. Barrio-Conde, M. A. Zanella, J. M. Aguiar-Perez, R. Ruiz-Gonzalez, and J. Gomez-Gil, "A deep learning image system for classifying high oleic sunflower seed varieties," *Sensors*, vol. 23, no. 5, p. 2471, 2023.

[27] J. Zhang, L. Dai, and F. Cheng, "Classification of frozen corn seeds using hyperspectral VIS/NIR reflectance imaging," *Molecules*, vol. 24, no. 1, p. 149, 2019.

[28] K. Tan, Y. Chai, W. Song, and X. Cao, "Identification of soybean seed varieties based on hyperspectral image," *Transactions of the Chinese Society of Agricultural Engineering*, vol. 30, no. 9, pp. 235–242, 2014.

[29] M. Huang, C. He, Q. Zhu, and J. Qin, "Maize seed variety classification using the integration of spectral and image features combined with feature transformation based on hyperspectral imaging," *Applied Sciences*, vol. 6, no. 6, p. 183, 2016.

[30] J. Zhang, L. Dai, and F. Cheng, "Corn seed variety classification based on hyperspectral reflectance imaging and deep convolutional neural network," *Journal of Food Measurement and Characterization*, vol. 15, no. 1, pp. 484–494, 2021.

[31] X. Chu, H. Yuan, and W. Lu, "Progress and application of spectral data pretreatment and wavelength selection methods in NIR analytical technique," *Progress in Chemistry*, vol. 16, no. 04, p. 528, 2004, https://manu56.magtech.com.cn/progchem/EN/abstract/abstract8972.shtml.

[32] C. Alamprese, M. Casale, N. Sinelli, S. Lanteri, and E. Casiraghi, "Detection of minced beef adulteration with Turkey meat by UV–vis, NIR and MIR spectroscopy," *LWT--Food Science and Technology*, vol. 53, no. 1, pp. 225–232, 2013.

[33] F. Hu, M. Zhou, P. Yan et al., "Selection of characteristic wavelengths using SPA for laser induced fluorescence spectroscopy of mine water inrush," *Spectrochimica Acta Part A: Molecular and Biomolecular Spectroscopy*, vol. 219, pp. 367–374, 2019.

[34] D. Liu, D. W. Sun, and X. A. Zeng, "Recent advances in wavelength selection techniques for hyperspectral image processing in the food industry," *Food and Bioprocess Technology*, vol. 7, no. 2, pp. 307–323, 2014.

[35] M. Ye, L. Zhu, X. Li et al., "Estimation of the soil arsenic concentration using a geographically weighted XGBoost model based on hyperspectral data," *Science of The Total Environment*, vol. 858, Article ID 159798, 2023.

[36] W. He, H. He, F. Wang et al., "Rapid and uninvasive characterization of bananas by hyperspectral imaging with extreme gradient boosting (XGBoost)," *Analytical Letters*, vol. 55, no. 4, pp. 620–633, 2022.

[37] Y. Shang, X. Zheng, J. Li, D. Liu, and P. Wang, "A comparative analysis of swarm intelligence and evolutionary algorithms for feature selection in SVM-based hyperspectral image classification," *Remote Sensing*, vol. 14, no. 13, p. 3019, 2022.

[38] J. Zhang, L. Dai, and F. Cheng, "Identification of corn seeds with different freezing damage degree based on hyperspectral reflectance imaging and deep learning method," *Food Analytical Methods*, vol. 14, no. 2, pp. 389–400, 2021.

[39] Y. LeCun, L. Bottou, Y. Bengio, and P. Haffner, "Gradient-based learning applied to document recognition," *Proceedings of the IEEE*, vol. 86, no. 11, pp. 2278–2324, 1998.

[40] C. Szegedy, W. Liu, Y. Jia et al., "Going deeper with convolutions," in *Proceedings of the IEEE Conference on Computer Vision and Pattern Recognition*, pp. 1–9, IEEE, 2015, https://www.cv-foundation.org/openaccess/content_cvpr_2015/papers/Szegedy_Going_Deeper_With_2015_CVPR_paper.pdf.

[41] K. He, X. Zhang, S. Ren, and J. Sun, "Deep residual learning for image recognition," in *Proceedings of the IEEE Conference on Computer Vision and Pattern Recognition*, pp. 770–778, IEEE, Vancouver, Canada, June 2016, https://openaccess.thecvf.com/content_cvpr_2016/html/He_Deep_Residual_Learning_CVPR_2016_paper.html.

[42] S. Wakhid, R. Sarno, and S. I. Sabilla, "The effect of gas concentration on detection and classification of beef and pork mixtures using E-nose," *Computers and Electronics in Agriculture*, vol. 195, Article ID 106838, 2022.

[43] T. Deák, Z. Seregély, K. J. Kaffka, E. Bába, V. Zarkaa, and G. D. Bisztraya, "Distinction of melon genotypes using NIR spectroscopy," in *Proceedings of the 11th International Conference on Near Infrared Spectroscopy*, pp. 385–388, IEEE, Cordoba, Spain, 2004, https://www.researchgate.net/profile/Tamas_Deak/publication/267830070_Distinction_of_melon_genotypes_using_NIR_spectroscopy/links/55911b4908aed6ec4bf69176/Distinction-of-melon-genotypes-using-NIR-spectroscopy.pdf.